Experimental Study of Flow Regimes in Three-Dimensional Confined Impinging Jets Reactor

Wei-Feng Li, Ke-Jiang Du, Guang-Suo Yu, Hai-Feng Liu, and Fu-Chen Wang
Key Laboratory of Coal Gasification and Energy Chemical Engineering of Ministry of Education, East China University of Science and Technology, Shanghai 200237, China

DOI 10.1002/aic.14459
Published online April 8, 2014 in Wiley Online Library (wileyonlinelibrary.com)

Dynamic behaviors in a three-dimensional confined impinging jets reactor (CIJR) were experimentally studied by a flow visualization technique at $100 \leq Re \leq 2000$ and $2 \leq D/d \leq 12$ (where D is the reactor diameter and d is the nozzle diameter). The effects of inlet Reynolds numbers (Re) and geometry configurations of the CIJR on the flow regimes have been investigated by a particle image velocimetry and a high-speed camera. Results show that with the increasing Re, a segregated flow regime, a radial deflective oscillation, an axial oscillation and a vortex shedding regime emerge in turns in CIJR. A map of parameter space formed by the inlet Reynolds number (Re) and the normalized reactor diameter (D/d) has been presented. The effects of jet instability and confined boundary of the chamber on the flow regimes and their transition are also investigated and discussed. © 2014 American Institute of Chemical Engineers *AIChE J*, 60: 3033–3045, 2014

Keywords: confined impinging jets reactor, mixing, oscillation behaviors, reactor analysis

Introduction

As impinging jets can intensify transfer and mixing processes effectively, they have been widely and successfully applied to more and more industrial processes, for example, the rapid fluids mixing or chemical reaction, the gasification or combustion, the extraction or absorption, the polymer and nanoparticle synthesis.[1–4] So far, most studies about the impinging jets reactor are about T-jets mixer and confined impinging jets reactors (CIJR) with miniscale or microscale. The advance and state of the mini/micro impinging jets reactors were well reviewed lately by Santos and Sultan,[5] and they have pointed out that scaling-up the reactor with the aim to increase its throughput is a challenging task, because scaling-up will compromise the mixing effect. Current fundamental studies of CIJR are not enough for their scaling-up and increasing industrial applications.

A main difficulty for the study of impinging jets reactor is the factors affecting the flow regime are numerous, for example, jet Reynolds numbers, geometry configurations, and inlet boundary conditions. In last three decades, many types of CIJR have been intensively investigated by experimental measurements and numerical simulations.[6–22] CIJR has been used in reaction injection moulding (RIM) for mixing of two reactive monomers to produce polymers. Typically, RIM mixing chambers are cylindrical from top to outlet, and have two opposed injectors with a diameter of about 1 mm and the normalized chamber diameter (D/d, where D is the reactor diameter and d is the nozzle inner diameter) is 6.67,[8–12] while the CIJR used for chemical reaction has a spherical top and a conical constriction at the outlet and the normalized reactor diameter is about 4.78.[16–18] Most of these studies have observed the transition from a segregated steady flow to a dynamic chaotic flow above Reynolds numbers of 100 in their experiments. The dynamic flow regime is characterized by the formation of a pancake-like structure above the critical Reynolds number and the flow oscillates with a complex mode.

Wood et al.[6,7] investigated the flow field created by two impinging liquid jets in a cylindrical chamber using particle tracing, laser Doppler anemometry (LDA), and three-dimensional (3-D) numerical simulation at $50 \leq Re \leq 300$. They observed an asymmetric oscillation at Re around 120, and the jet impingement point moved off-center and the jets no longer impinged on one another at $Re > 150$.[6] They classified this oscillation in RIM as a kind of self-sustained oscillation.[7] For the flow in RIM at $50 \leq Re \leq 600$, Santos et al.[8,9] found the transition from a stable laminar to a self-sustainable chaotic flow regime at $Re \approx 120$ using particle image velocimetry (PIV), and the Strouhal number (St) was in the range of 0.004–0.04 by LDA measurement of the velocity fluctuation near the impingement point. Their measurements indicate that the flow system is not oscillating with a single frequency but rather within a range of typical frequencies, and the flow regime in RIM is chaos at $Re > 120$, especially at $Re > 250$. To explain the oscillation behavior, they suggested that the jets impingement point was vibrating at the same frequency of the vortices formation rate and found the Strouhal numbers were affected by the geometry configuration of mixing chamber significantly.[10] Zhao and Brodkey[21] observed large-scale, 3-D unsteady motions in the opposed jets mixers using particle tracking velocimetry.

Correspondence concerning this article should be addressed to W.-F. Li at liweif@ecust.edu.cn.

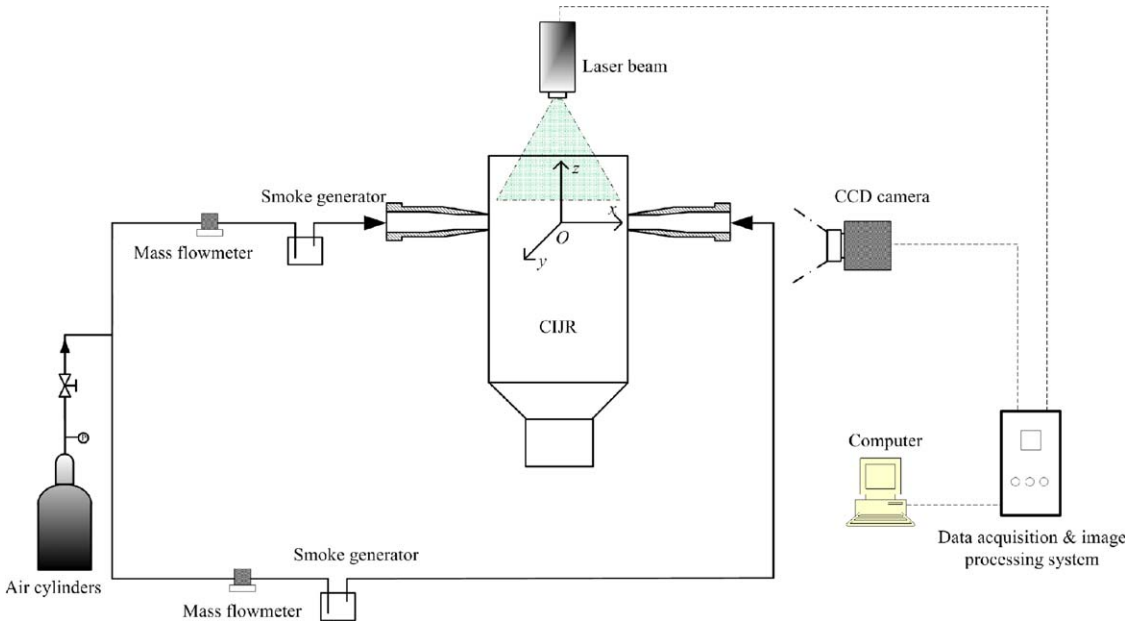

Figure 1. Schematic plan of experimental flow chart.

[Color figure can be viewed in the online issue, which is available at wileyonlinelibrary.com.]

Icardi et al.[17] observed the impingement plane was periodically broken in many smaller eddies at $Re = 310$, and the flow was fully chaotic for $Re = 600$, and the impingement plane was rarely imaged in the chamber center, whereas in most images it was replaced by many small eddies that interact with the incoming jets streams. Unger and Muzzio[22] observed that when the Reynolds number was increased to 200, a direct impingement was no longer possible, and the frequency and amplitude of jet oscillations continuously increased. It can be seen from above studies that the flow regimes at $Re > 200$ are very chaotic and complex, but the underlying reasons are still unknown.

Numerical simulations were also applied aiming at a better understanding of the inner mechanisms of the mentioned flow regimes by both 2-D and 3-D computational fluid dynamics (CFD) simulations, steady solving and unsteady solving, and RANS, LES, and DNS.[12,14–20,23,24] It should be mentioned that Icardi et al.[17] have investigated the flow field in a 3-D CIJR by means of microPIV and DNS. They have pointed out that oscillations present in the inlet flow of the device enhance the chaotic and turbulent effects in the reactor, and some small excitation oscillations similar to the experimental ones should be introduced in inflow conditions in DNS to obtain simulations consistent to experimental measurements.[17] This special treatment of the inlet boundary conditions implies that the disturbance in the inlets has a significant effect on the flow regimes in CIJR and should be considered in the simulation.

Due to the effect of confined boundary condition, the flow regime of the self-sustained oscillation in CIJR is basically different to the stagnation point offset of unrestricted axisymmetric opposed jets, which has been extensively studied in our previous studies.[25–27] We have found that there exists a range of $2 \leq L/d \leq 8$ (where L is the nozzle separation and d is the jet diameter), in which the stagnation point is very sensitive to the exit velocity ratio of the opposed jets.[25] The effect of the confined boundary condition on the flow regime in CIJR has not been revealed yet.

In spite of the fact that the dynamic behavior in CIJR has been observed for a long time, the underlying mechanism responsible for this complex dynamics has remained, to a large extend, unexplored. Motivated by the contributions of earlier studies, we present a fundamental study of the flow regimes in the CIJR at $100 \leq Re \leq 2000$ and $2 \leq D/d \leq 12$ in this article. The effects of jet Reynolds numbers, geometry configurations, and confined boundary conditions on the flow regimes were investigated using a flow visualization technique combining with a PIV system and a high-speed camera. Current work aims to get new insights on the complicated dynamic behaviors and the intrinsic mechanics of opposed jets in a CIJR. For simplicity, the impinging jets reactors with various geometry configurations are abbreviated as CIJR in the subsequent sections of current article.

Experimental Methods

Experiment setup and flow visualization

The schematic setup is drawn in Figure 1. Air was supplied by an air cylinder after pressure reduction. The bulk fluxes of the airflows to the nozzles were controlled by two mass flow meters with accuracy of $\pm 0.25\%$ of full scale deflection. The flow field of confined opposed jets was obtained by two identical axisymmetric nozzles installed on a cylindrical chamber. The instantaneous flow patterns in the CIJR were visualized by the white smoke generated by some small fuming tablets. As shown in Figure 1, the tablets were placed in the smoke generators and the generated smoke was carried into the flow field. In the experiment, the smoke was introduced to only one jet in order to observe the shape and location of the impingement plane more clearly.

The visualization images were captured by a PIV system and a high-speed camera. The CCD camera of the PIV system yielded vivid and clear sliced pictures of the flow patterns, but the pair of pictures were acquired by a frequency of 10 Hz due to the limitation of the pulsed laser. The acquired speed of high-speed camera can reach 1000 fps

Table 1. Summary of Experimental Conditions and Parameters

Item	Symbol	Value
Inner diameter of the reactor chamber (mm)	D	50
Normalized nozzle separation	D/d	$2 \sim 12$
Mean bulk velocity at the nozzle exit (m/s)	u_0	$0.06 \sim 7.12$
Jet Reynolds number $(du_0\rho/\mu)$	Re	$100 \sim 2000$

easily, but the captured images were blurred, so it was used to analyze the movement of the impingement plane under larger jet velocities and to validate the results of PIV. The recorded digital images were analyzed by the NIH Image freeware to obtain the oscillation frequencies, oscillation amplitudes or oscillation angles of the dynamic behavior of the impingement plane. The detailed method of the image processing can be found in our previous article.[28,29]

The summary of the experimental cases of the flow visualization is listed in Table 1. The schematic of the CIJR and the definition of the coordinate system are plotted in Figure 2. The chamber diameters (D) were 50 ± 0.02 mm and the chamber diameters normalized by the nozzle exit diameter (D/d) were in the range of 2–12. The normalized height from nozzle plane to the dome (h/d) was in the range of 0.5–1.25. The bulk mean velocities (u_0) at the nozzle exits were in the range of 0.06–7.12 m/s, and the corresponding jet Reynolds numbers ($du_0\rho/\mu$) were in the range of 100–2000.

PIV system

The images of the smoke-seeded flow were captured by the CCD camera of a PIV system (Dantec) consisting of a twin second harmonic Nd-YAG laser system ($\lambda = 532$ nm, pulse energy 200 mJ, and pulse frequency 10 Hz) and an image processor (Dantec Dynamic Studio). The laser "sheet" of a thickness of 1 mm was formed from the Nd-YAG laser beam by a light guide arm. The area of the measured flow field was 15×15 cm^2. The images of the smoke following the flow in the laser "sheet" were recorded by a CCD camera (FlowSense EO 4M camera). The captured images were transmitted by the image processor to a PC computer.

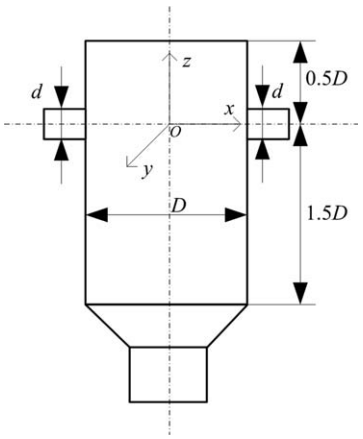

Figure 2. Schematic plan of dimensions of CIJR.

High-speed camera

A high-speed camera (Photron, APX-RS, up to 3000 frames per second with full resolution of 1024×1024 pixels) combined with a continuous 2000 W direct current light were also used to capture the instantaneous images of the smoke-seeded flow. The exposure time was set to 0.001 s and the instantaneous images were photographed with a frame rate of 1000 frames per second and resolution of 1024×1024 pixels.

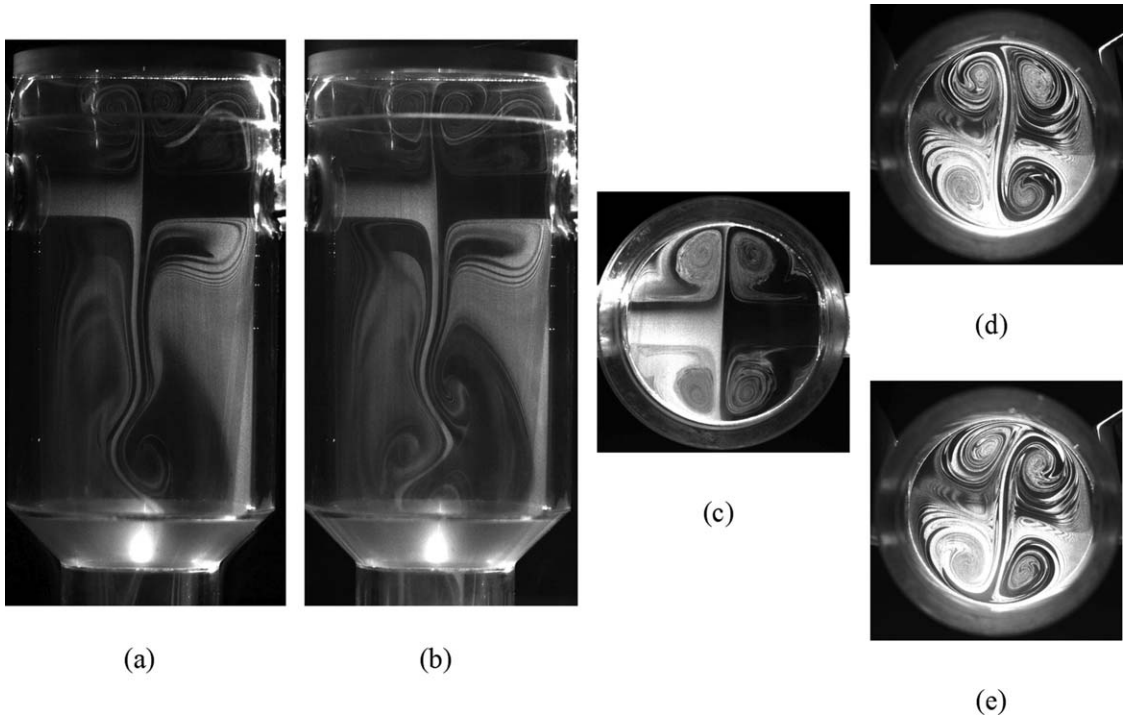

Figure 3. Instantaneous snapshots imaged by CCD camera at $Re = 100$ and $D/d = 4.8$.

(a), (b) $y = 0$ plane; (c) $z = 0$ plane; (d), (e) $z = -25$ mm plane.

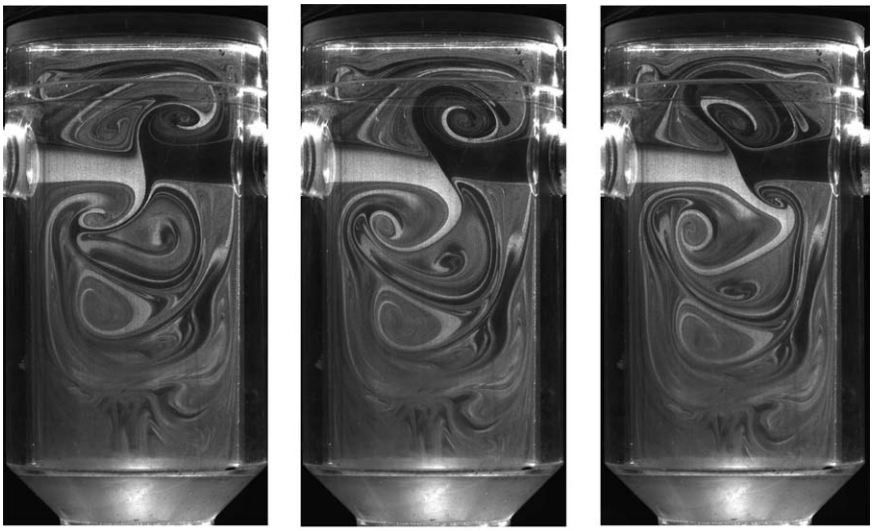

(a) $t=t_0$ (b) $t=t_0+0.1$ s (c) $t=t_0+0.2$ s

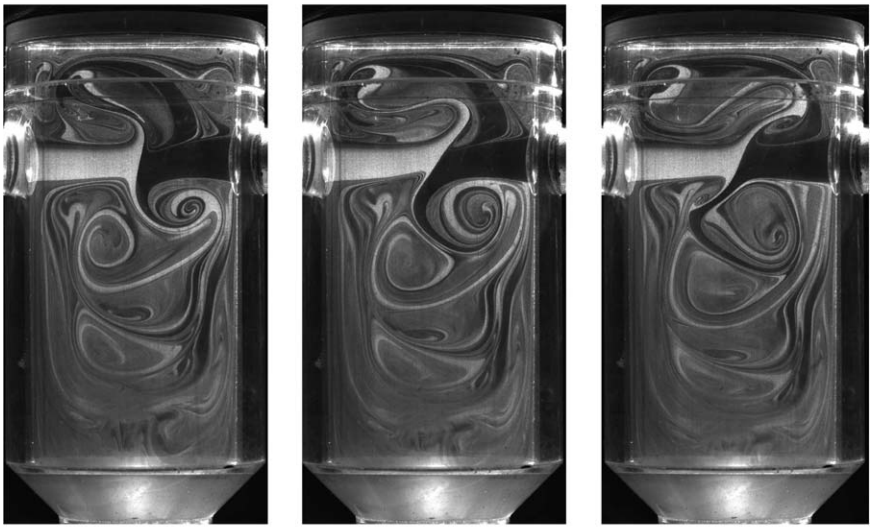

(d) $t=t_0+0.3$ s (e) $t=t_0+0.4$ s (f) $t=t_0+0.5$ s

Figure 4. Instantaneous snapshots imaged by CCD camera in $y=0$ plane at $Re=150$ and $D/d=4.8$.

Results

Flow regimes in CIJR

The Segregated Flow Regime. Some typical instantaneous slices of smoke-seeded flow patterns at $Re=100$ are presented in Figure 3. It can be seen that by collisions, the opposed jets form an impingement plane with a "pancake" shape, and axial round jets change to a thin radial jet. Figure 3 also indicates that the center part of the impingement is stable and exhibits a segregated flow regime, but the upper and the lower parts twist periodically in their plane. The occurrence of this flapping oscillation is due to the interaction of the impingement plane with the chamber walls.

The Radial Deflective Oscillation. About at $Re=150$, a flow regime characterized by the deflective oscillation of the radial jets is identified, and is called a "radial deflective oscillation." As shown in Figure 4, this kind of deflective oscillation displays S-shaped and changes its directions in their planes periodically. The images in $z=0$ plane also exhibit a deflective oscillation and its period is nearly equal to that of $y=0$ plane, as shown in Figure 5. The visualization results in Figures 4 and 5 prove the dynamic behavior in CIJR is a kind of self-sustained oscillation with 3-D and antisymmetric characteristics. It should be pointed out that the Re corresponding to the radial deflective oscillation is in the narrow range of $150 \le Re < 300$. The upper and lower limits of this range are difficult to precisely determine because they are affected by the geometry configurations of the reactor and the disturbances in the experiment.

A Transition from Radial Deflective Oscillation to Axial Oscillation. With the increasing Re to about 300, the radial deflective oscillation becomes irregular and the axial oscillation of the impingement plane is pronounced. The flow in CIJR displays a hybrid regime of radial deflective oscillation and axial oscillation, as shown in Figure 6. The Re range corresponding to this hybrid regime is $300 \le Re \le 500$. With increase of Re, the flow regime shows a transition from

(a) $t=t_0$ (b) $t=t_0+0.1$ s (c) $t=t_0+0.2$ s

(d) $t=t_0+0.3$ s (e) $t=t_0+0.4$ s (f) $t=t_0+0.5$ s

Figure 5. Instantaneous snapshots imaged by CCD camera in $z = 0$ plane at $Re = 150$ and $D/d = 4.8$.

radial deflective oscillation to axial oscillation. Just as reviewed in the introduction, the flow in CIJR at $300 \leq Re \leq 500$ is categorized as a chaotic flow regime, and the disappearance of the impingement plane has been reported by some researchers.[17,22] For our results, the impingement plane is visible in most times, but the disappearance of the impingement plane has also been observed occasionally. By many attempts of experiments, we have found the chaotic flow results from the substantial fluctuation in the inflow of the jets or the misalignment of the two nozzles along the symmetry axis. The increasing axial instability of the impingement plane is the main cause of the chaotic flow in CIJR.

Hybrid of Axial Oscillation and Vortex Shedding Regimes. At $Re > 500$, the axial oscillation of the impingement plane becomes more irregular, and a new flow regime characterized by the vortex shedding in the impingement plane is observed, as shown in Figure 7. With the increasing Re, the vortex shedding regime is pronounced with the increasing antisymmetric waves on the impingement plane caused by collision instability in the stagnation point. The vortex shedding makes the impingement plane decay after a certain distance away from the impingement point, which is beneficial to the fluid mixing in CIJR. At $Re > 1000$, it is very difficult to get the impingement point located at the midpoint between the nozzles, and the impingement plane tends to locate at the positions near to the two nozzles, which is similar to the stagnation point offset studied in our previous works.[25–27]

Analysis of the images at different Reynolds numbers

The time series of axial oscillation of impingement plane and deflective angles of the radial directions obtained from visualization images were analyzed by NIH software. The time histories of the locations of the impingement plane on the axis are presented in Figure 8, in which the data are obtained from the images captured by the CCD camera with a frequency of 10 Hz. It can be seen that the axial oscillation is absent at $Re = 100$, and its oscillation amplitude is relatively small at $150 \leq Re < 300$, but increases sharply at $Re \geq 300$. Generally, the axial oscillation is irregular and has a low frequency on the order of 1 Hz, but has large amplitude on the order of the chamber diameter.

If the normalized location of the stagnation point on the axis at time i is x_i, the root mean square (rms) of the time history is defined as follows to indicate the degree of the axial oscillation

$$\mathrm{rms} = \sqrt{\overline{\sum_{i=0}^{t_0} x_i^2}} \tag{1}$$

where t_0 is the statistical time. The rms of the time history of the stagnation point on the axis is shown in Figure 9, in which the statistics time of each data is 12 s. It can be seen that rms increases rapidly, especially at $Re < 500$, which indicates the axial oscillation of the impingement plane was pronounced with Re. The rms values obtained by the CCD camera and the high-speed camera are generally in agreement and some difference occurs at $Re > 1000$. Considering the difference of the acquiring frequency of the two techniques, the results obtained by the high-speed camera should be more credible at $Re > 1000$.

Compared to the analysis of the axial oscillation, the analysis of the radial deflective oscillation is somewhat difficult. In the experiments, we have observed that the upper part, the lower part, and the center part of the impingement plane have different deflecting angles, so they must be analyzed, respectively. The definitions of the deflecting angles of the three parts of the impingement plane are shown in Figure 10. The position of the stagnation plane on the axis is x_i,

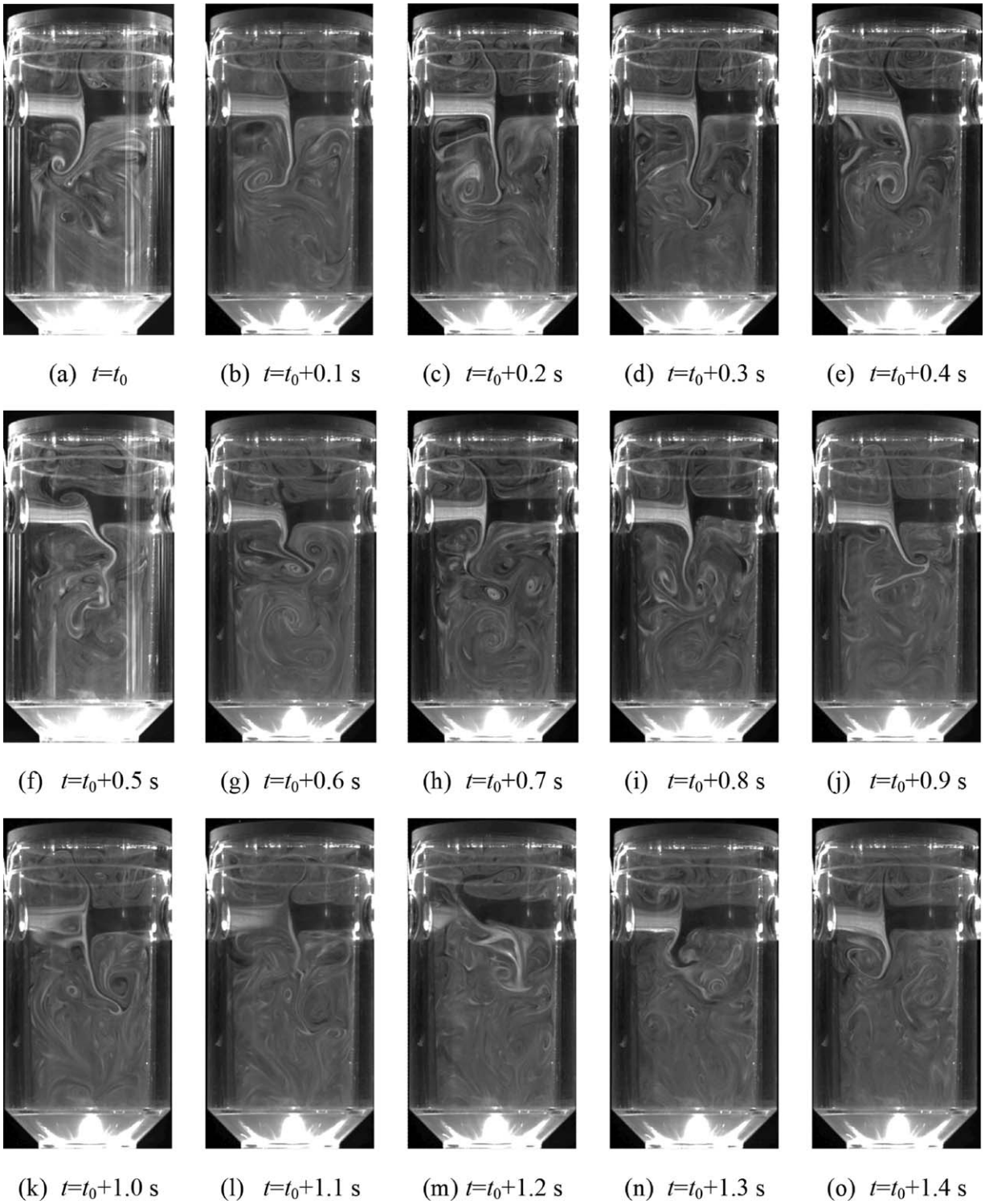

Figure 6. Instantaneous snapshots imaged by CCD camera in $y = 0$ plane at $Re = 300$ and $D/d = 4.8$.

and the line y' is through the stagnation point and parallel to y-axis. In the figure, θ_1 is the angle between the center part of the impingement plane and line y', and θ_2 is the angle between line y' and the line from the stagnation point to the vortex core of the upper part of the impingement plane, and θ_3 is the angle between line y' and the line from the stagnation point to the vortex core of the lower part of the impingement plane.

The time series of the deflecting angles of the three parts of the impingement plane are presented in Figure 11, in which the data are obtained from the images captured by the CCD camera of the PIV system with a frequency of 10 Hz. At $Re = 100$, the center part of the impingement plane does not deflect and oscillate, but the upper and lower part show regular deflective oscillation due to the interactions of the impingement plane with the dome and the conical outlet of

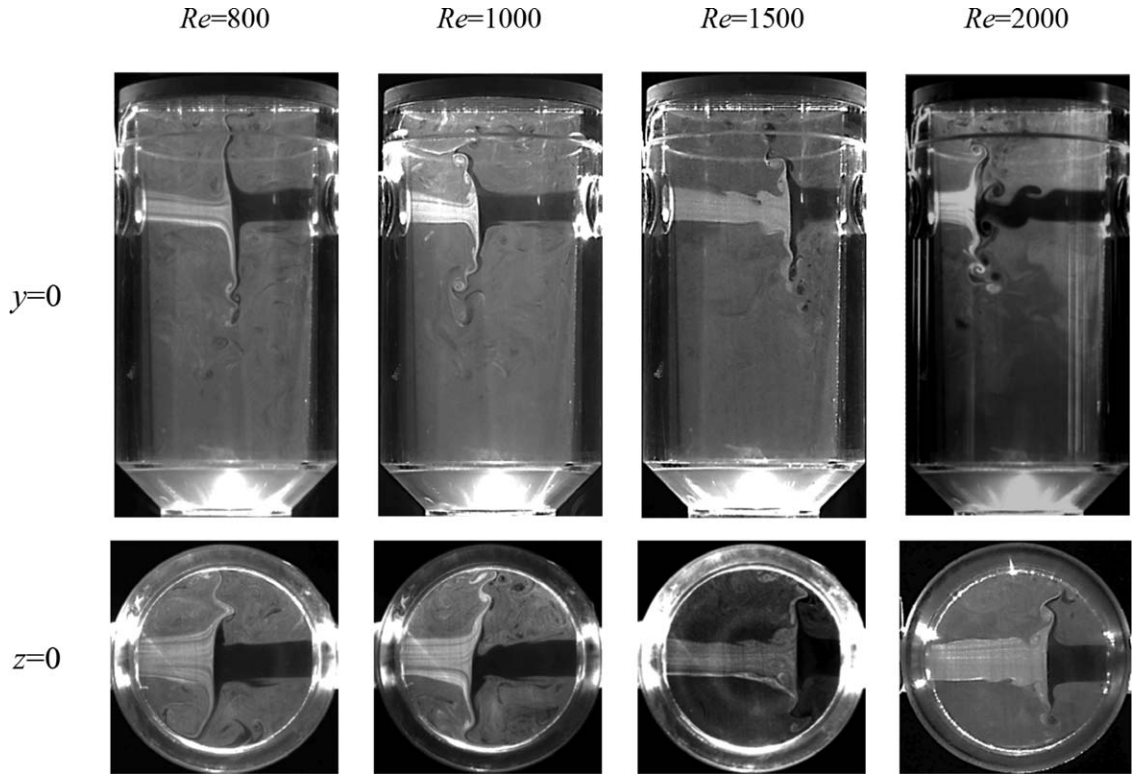

Figure 7. Instantaneous snapshots imaged by CCD camera at $D/d = 4.8$ and $500 < Re \leq 2000$.

the chamber, as shown in Figure 3. At $Re = 150$, all the three parts of the impingement plane show relatively regular deflective oscillations and the mean oscillation periods are all about 0.56 s. At $Re \geq 200$, the center part of the impingement plane shows an intermittent deflective oscillation, but the upper and the lower parts still oscillate continuously. About at $300 \leq Re \leq 500$, the deflective oscillations of the upper and the lower parts become irregular. At $Re > 500$, the deflective oscillations of the upper and the lower parts become more irregular but weak and are replaced by the vortex shedding of the impingement plane.

Here, an intermittency factor (I) of the radial deflective oscillation of the center part of the impingement plane is defined as

$$I = 1 - t_d/t_0 \tag{2}$$

where t_d is the time of the impingement plane with the radial deflective oscillation, and t_0 is the statistical time. The results of the analyzed intermittency factors are shown in Figure 12, in which the statistics time of each data is 12 s. The intermittency factor has minimum value at $Re = 150$, and increases rapidly with Re in the range of 150 to 1000. The intermittency factors analyzed from the images acquired by the CCD camera of the PIV system and the high-speed camera generally show the same trend, and only at $Re \geq 1000$, the intermittency factors from images acquired by the CCD camera are somewhat smaller than those of high-speed camera. As the PIV system with a low acquiring frequency of 10 Hz is not enough to capture the detail of the radial deflective oscillation at high Re, the results obtained by the high-speed camera are more trusted at $Re \geq 1000$.

The Strouhal number (St) of the radial deflective oscillation is defined as

$$St = fd/u_0 \tag{3}$$

where f is the frequency of the radial deflective oscillation analyzed from the images acquired by the CCD camera, d is the jet diameter, and u_0 is the initial jet velocity. The Strouhal numbers of radial deflective oscillations of the upper and lower parts of the impingement planes at $D/d = 4.8$ are shown in Figure 13, in which each value is the statistical average of 15 oscillation periods and the error bars mark the standard deviation of the data. It can be seen that the difference of the radial deflective oscillation of the upper and lower parts is insignificant. Except for $Re = 100$, the error bars of the radial deflective oscillation are high, which indicates this kind of oscillation is not regular. Strictly speaking, only oscillations in the range of 150–200 can be classified to a regular and self-sustained oscillation. At $Re > 200$, the increasing axial instability makes the radial deflective oscillation become more and more irregular.

The Strouhal numbers of the deflective oscillation of the upper parts of the impingement planes at $D/d = 4.8$ and 6.67 are presented in Figure 14, in which the results in the literature are also added for comparison.[7,8] With increase of normalized reactor diameter, the Strouhal number decreases, and the Strouhal numbers increase rapidly at $Re < 150$ and the maximum values appear at about $Re = 150$. At $Re > 150$, the Strouhal numbers decrease slowly and are about 0.04 at $D/d = 6.67$. Due to the differences of the jet velocities and jet diameters, the oscillation frequencies in current work are in the range of 1–5 Hz, while the peak frequencies in the work of Santos and coworkers[8] are in the range of 100–300 Hz. Although the work fluids are gas and liquid, the Strouhal numbers in current work are in good agreements with their results at $D/d = 6.67$. Results reported by Johnson and Wood[7] indicate that the Strouhal numbers decrease with chamber diameters but increase with Reynolds numbers under

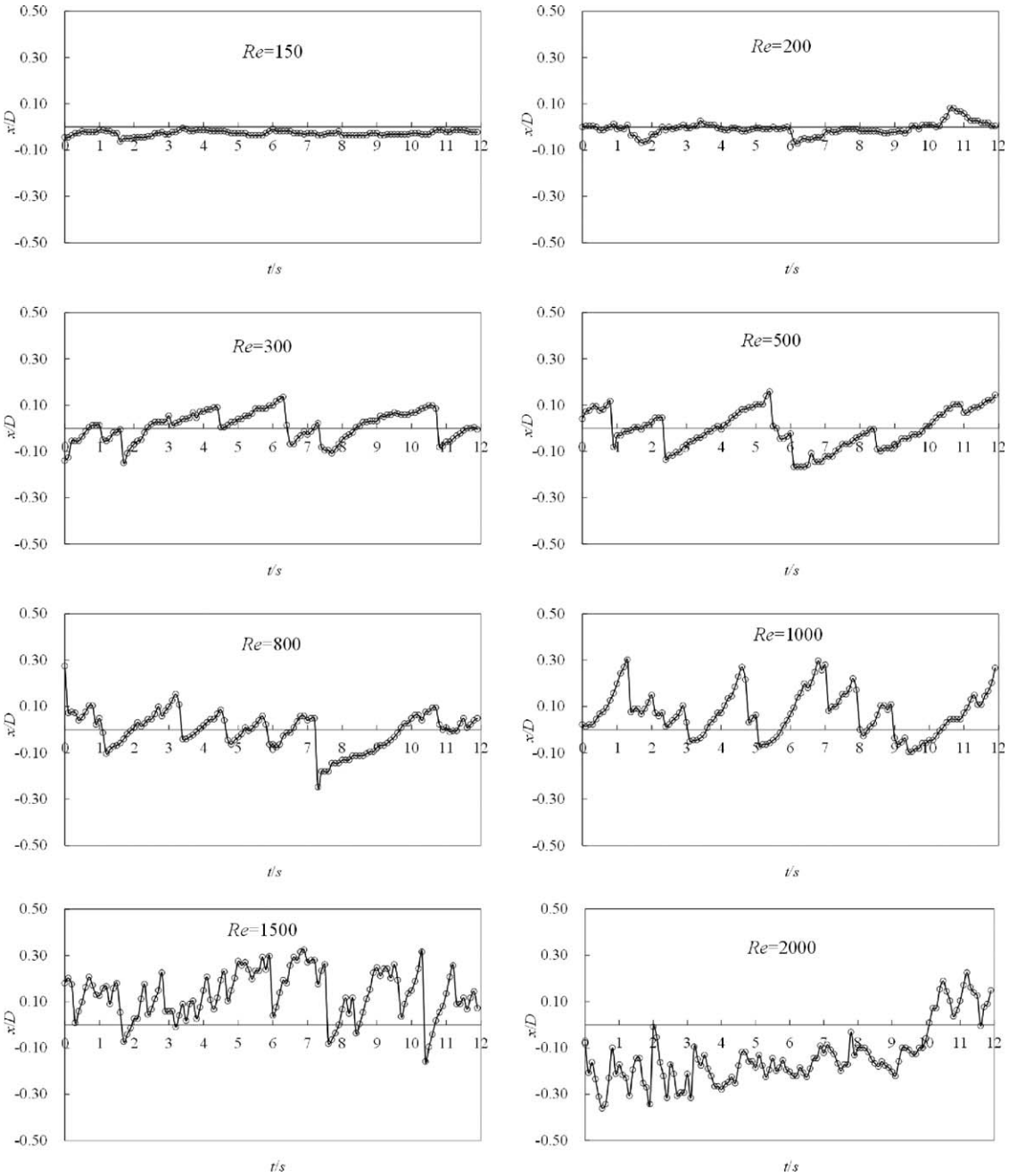

Figure 8. Time history of position of the stagnation point on the axis at $D/d = 4.8$.

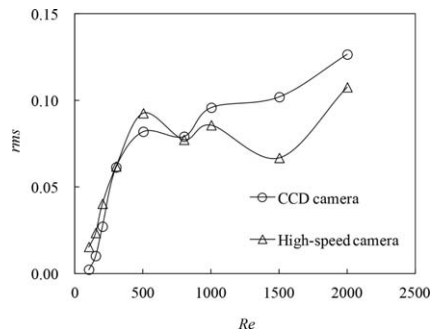

Figure 9. The rms of the time history of the stagnation point on the axis at $D/d = 4.8$.

their experimental conditions, which is in general agreement with the conclusion in current work. While the Strouhal numbers in the work of Johnson and Wood[7] are somewhat smaller than those of current work and Santos and coworkers[8] which is maybe due to the differences of the geometry configurations of the mixing chambers and Reynolds numbers. Earlier comparisons prove that the flow regimes of CIJR in these works are same in essence and the oscillation behaviors are mainly determined by the geometry configurations of the mixing chambers and Reynolds numbers.

The effect of geometry parameters on the flow regime in CIJR

In our experiments, the effects of geometry parameters, such as the shape of the dome (plane and hemispheric) and

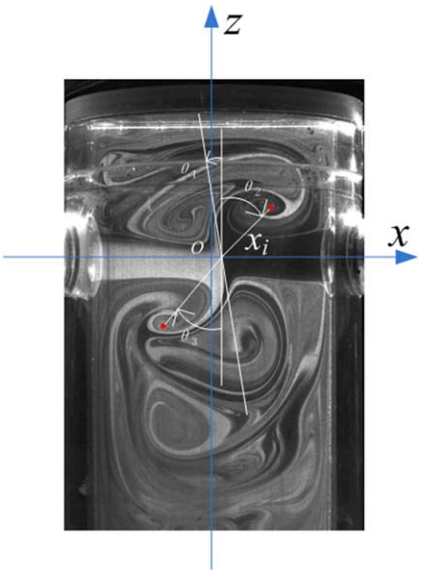

Figure 10. Definition of the deflective angles of the curved impingement plane.

[Color figure can be viewed in the online issue, which is available at wileyonlinelibrary.com.]

the chamber (round and square), the height from the nozzle plane to the dome ($h/D = 0.5$, 1, and 1.25) and normalized chamber diameter ($D/d = 2$, 4.8, 6.67, and 12) on the flow regimes in CIJR have also been investigated preliminarily. The visualization images in CIJR with various geometry configurations are presented in Figure 15. Results show that the shape of the dome only has slight effect on the transition of the flow regimes from the separated flow to radial deflective oscillation. For the case of square chamber, the critical *Re* for the transition from the segregated flow regime to radial deflective oscillation increase to about 200, and the oscillation behavior at $Re > 200$ is similar to those of round chamber. At $h/D = 1$ and 1.25, the *Re* corresponding to the onset of the radial deflective oscillation also increases to about 200, and the oscillation behaviors are similar to the case of $h/D = 0.5$. It should be pointed out that current experiments only preliminarily investigate the effects of some geometry parameters on the transitions of the flow regimes, and the detailed effects of these parameters on the turbulence intensity and mixing dynamics in the reactor are out of the scope of current study.

Overall, among these geometry configurations, the effect of the normalized chamber diameter on the flow regime is more significant than the dome and the chamber shapes, and the height from nozzle plane to the dome. The flow regimes at $D/d = 4.8$ and 6.67 are similar, and the effect of normalized chamber diameter on the Strouhal numbers is shown in Figure 14. At $D/d = 12$, the onset *Re* of the radial deflective oscillation increases to about 200 and the oscillation is weak and irregular compared to the cases of $D/d = 4.8$ and 6.67. But for CIJR at $D/d = 2$, a more complicated and chaotic flow regime emerges with the increasing *Re*. At $Re \geq 300$, the opposed jets are staggered and the impingement plane disappears. With even higher *Re*, the flow in CIJR is fully chaotic and the oscillation is more intensive and irregular. The complicated flow regime in CIJR at $D/d = 2$ is due to the intensive interaction of the impingement plane with the confined boundary wall.

A map of the parameter space indicating different flow regimes arising in CIJR is plotted in Figure 16, in which the symbols denote the experimental measurements. It can be seen that the flow regimes in CIJR can be classified into six types. Region I is corresponding to a stable separated flow regime, and region II denotes the radial deflective oscillation, and region III is a hybrid regime of the radial deflective oscillation and axial oscillation. Region IV is a hybrid regime of axial oscillation and vortex shedding, and region V is a hybrid regime of stagnation point offset and vortex shedding regime, and region VI is a chaotic flow regime.

Discussion

From above results, the Reynolds numbers and the confined boundary of the chamber are the dominant factors determining the flow regimes in CIJR. So the effects of jet Reynolds number and the confined boundary conditions on the origin and maintaining of the oscillation in CIJR are further investigated and discussed in this section.

The origin of the oscillation in CIJR

The first issue is the origin of the radial deflective oscillation which mainly appears at $150 \leq Re < 300$. There are some opinions about the causes of the oscillation regime in CIJR in the literature. The results of Santos et al.[10] indicated that in confined opposed jets mixers the jets impingement point oscillates with frequencies around typical values, and they presumed and confirmed that the oscillation frequency values are dictated by the geometry of the vortices occurring immediately downstream the jets impinging. Icardi et al.[17] have pointed out that only considering the natural instability generated by the impingement of the jets is not enough to explain the chaotic behavior in CIJR because the fluctuations present in the inlet flow of the device enhance the chaotic and turbulent effects in the reactor to a large extent. It can be seen that further explanations and discussion are very necessary for the complex flow regimes in CIJR.

To explain this problem, we suggest that first attentions should be focused on the instability of free jets with increasing *Re*. The effect of *Re* on opposed jets is related to onset of instabilities and growth of structures in the shear layer of jets. Many researchers have studied the instability evolution of low *Re* round jet.[30,31] They have observed that with increases of *Re* from several hundred to about 1000, the jets show the transition from a helical instability to axisymmetric instability, although there are discrepancies in various experimental studies regarding the Reynolds number at the onset of instabilities and the transition between them.[31] Our visualization results show that at $Re < 500$, the free round jets exhibit helical instability, as shown in Figures 17a,b, and at about $Re > 500$, the jets display axisymmetric instability, as shown in Figures 17c,d. So, when two low *Re* jets with helical instabilities impact oppositely, the impingement plane shows a radial defective oscillation. With the increase of *Re*, the jets display axisymmetric instability, and the flow regime in CIJR undergoes a transition from radial deflective oscillation to an axial instability.

Another explanation of the oscillation present in CIJR is the theory of self-sustained oscillation of impinging free shear layers.[32,33] According to this theory, the opposed jets impinge each other and create pressure disturbance in the impingement region near the stagnation point, which are fed back to the jets, continually forcing the oscillations.[32] With increasing Reynolds numbers in CIJR, the pressure disturbance and its feedback will increase, and the oscillation will be pronounced.

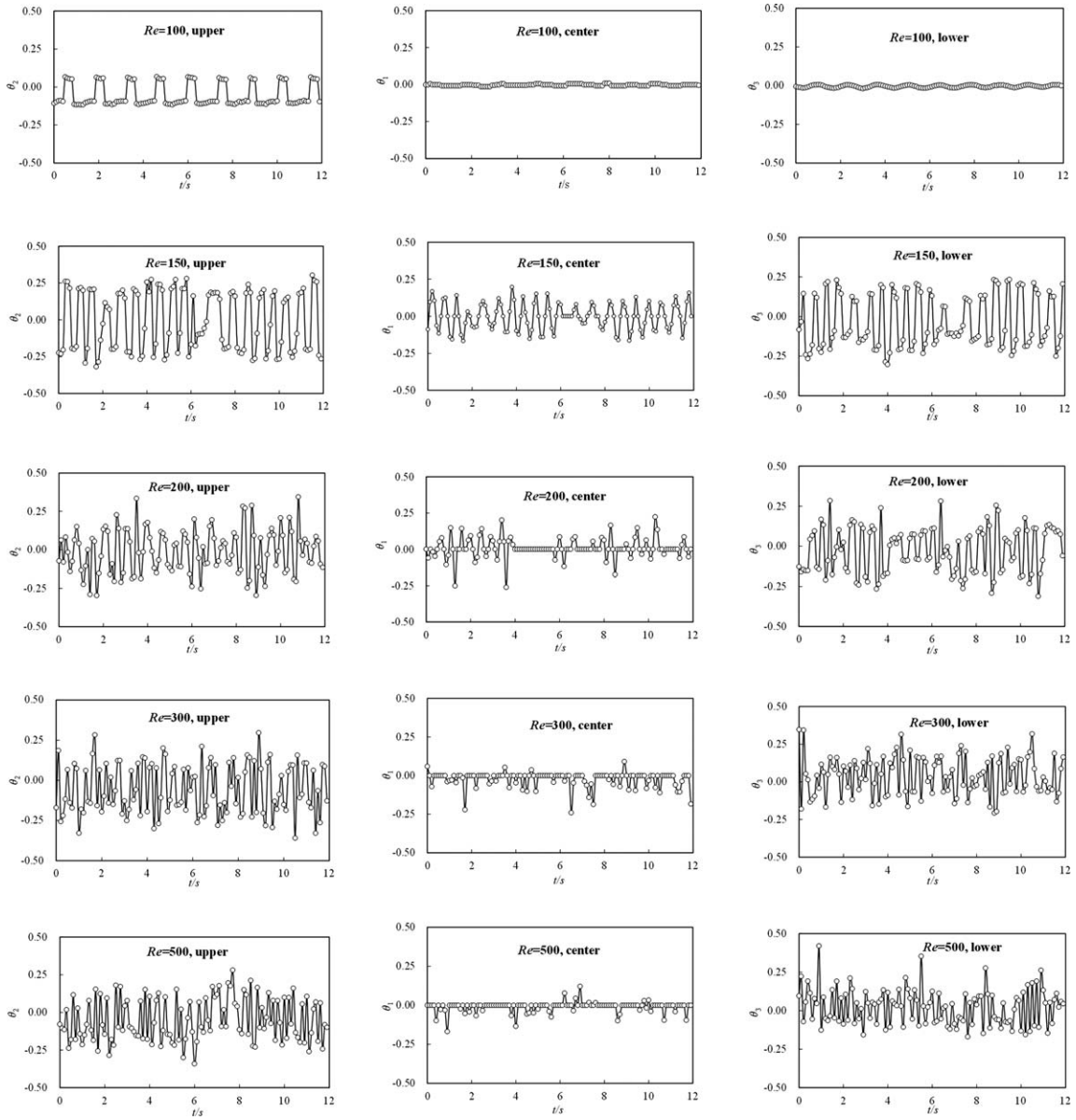

Figure 11. The time series of deflective angles of the impingement plane at $D/d = 4.8$.

The maintaining of the oscillation in CIJR

The second issue is how the oscillation in CIJR maintains? Above explanation about the natural instability of the free jets and the pressure disturbance and its feedback in the impingement region can address the onset of the oscillation and the transition from radial deflective oscillation to axial instability in CIJR with increasing Reynolds numbers, but they are not enough to explain the difference of the flow

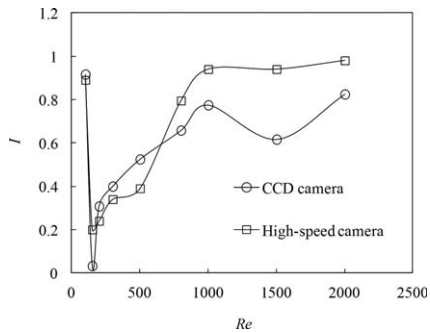

Figure 12. Values of intermittency factors of radial deflective oscillation in CIJR at $D/d = 4.8$.

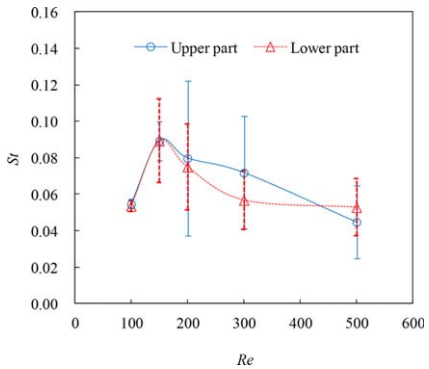

Figure 13. Evolution of the Strouhal number with the Reynolds numbers at $D/d = 4.8$.

[Color figure can be viewed in the online issue, which is available at wileyonlinelibrary.com.]

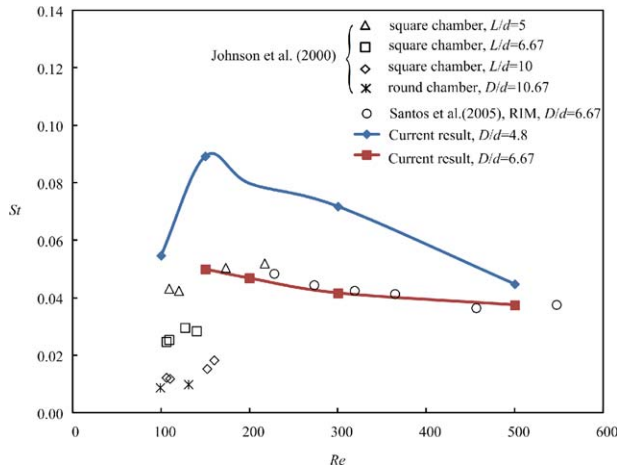

Figure 14. Values of *St* vs. *Re* in CIJR.

[Color figure can be viewed in the online issue, which is available at wileyonlinelibrary.com.]

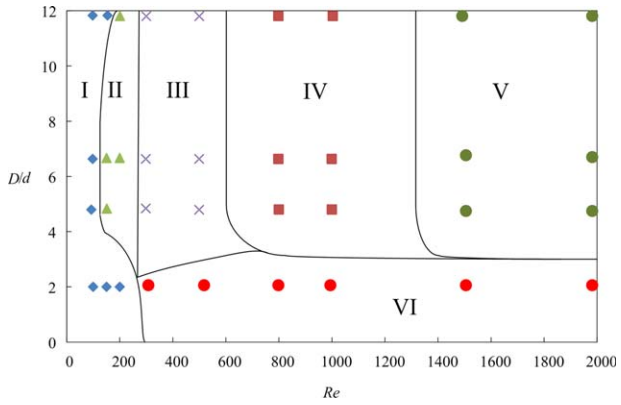

Figure 16. Map of the parameter space indicating different flow regimes arising in CIJR.

[Color figure can be viewed in the online issue, which is available at wileyonlinelibrary.com.]

regimes between the free and confined opposed jets. The visualization images of free opposed jets at $L = 4.8d$ (where L is the nozzle separation and d is the jet diameter) are shown in Figure 18, in which the nozzle configurations and nozzle separations are same to the CIJR. It can be seen that about at $Re \leq 500$, the impingement plane can locate at the center of the two nozzles, while at $Re > 500$, the impingement plane tends to locate in the positions near to the two nozzles, and axial oscillation of the impingement plane along the axis is occasionally observed due to the inflow fluctuations, which is similar to the stagnation point offset studied in our

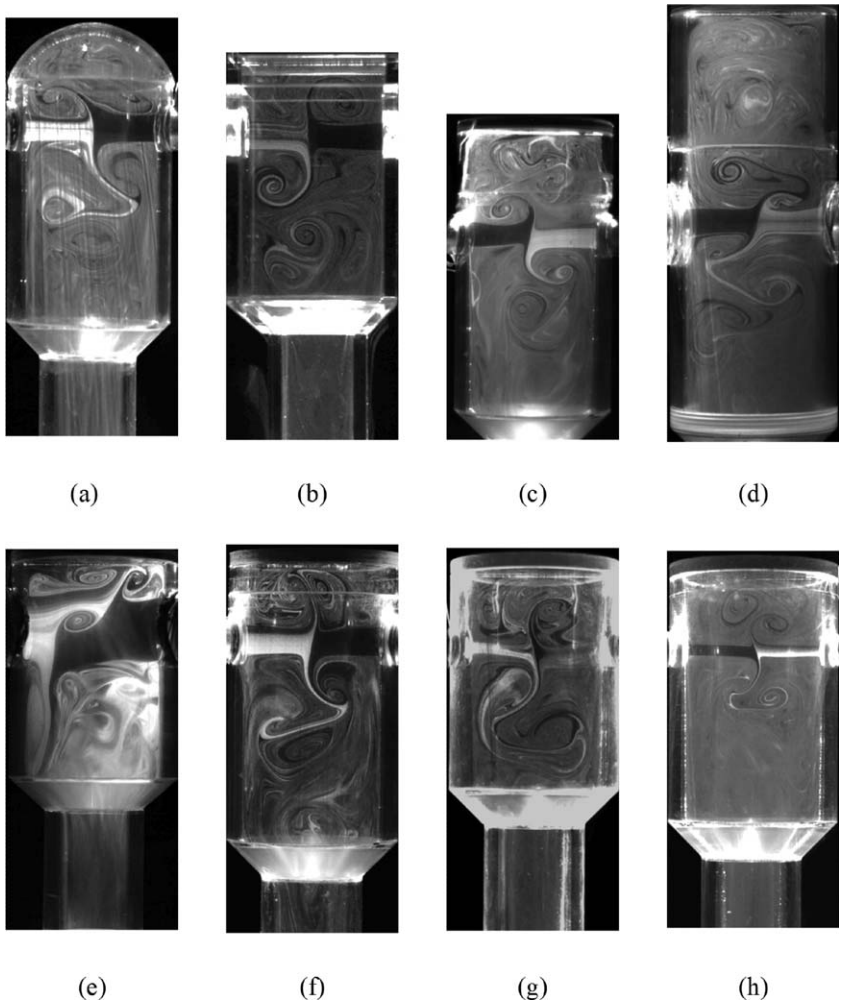

Figure 15. Instantaneous snapshots imaged by CCD camera in CIJR with different geometry configurations.

(a) $D/d = 4.8$, $Re = 150$, hemispheric dome and round chamber; (b) $D/d = 4.8$, $Re = 200$, square chamber and flat dome; (c) $D/d = 4.8$, $Re = 200$, and $h/D = 1$; (d) $D/d = 4.8$, $Re = 200$, and $h/D = 1.25$; (e) $D/d = 2$, $Re = 300$; (f) $D/d = 4.8$, $Re = 150$; (g) $D/d = 6.67$, $Re = 150$; (h) $D/d = 12$, $Re = 200$.

(a) *Re*=300 (b) *Re*=500 (c) *Re*=800 (d) *Re*=1500

Figure 17. Instantaneous snapshots of free round jets by CCD camera.

previous work.[25–27] For free opposed jets, the impingement plane is always vertical to the symmetry axis, and no deflective oscillation was observed. It should be pointed out that a deflective oscillation caused by the disturbance of the environmental airflow was occasionally observed at $Re = 100$. When the disturbance disappears, the impingement becomes vertical again, which implies the deflective oscillation can be induced by disturbance.

From the comparison between the flow regimes of CIJR and free opposed jets, one can see that the natural instability of the jets and pressure disturbance are not the dominant factors for the maintaining of the oscillation in CIJR, and we must consider the effect of the confinement of the chamber wall on the opposed jets. The oscillation in CIJR can be explained according to the self-sustained oscillation of a confined jet. Villermaux et al.[34] have pointed out that the self-sustained, quasiperiodic, and low frequency oscillation of the velocity and internal pressure of a confined jet comes from the confinement of walls, whose role is to establish a recirculation zone which convects large amplitude perturbations upstream. For the flow in CIJR, the destabilization of the impingement plane is originally caused by the natural instability of the jets and pressure disturbance in the impingement region, and the radial deflective oscillation of the impingement plane is caused by the recirculating zone formed by the confined boundary wall of chamber, as shown in Figures 4 and 5. Then the perturbations in the recirculating zone will push the deflecting oscillation of the impingement plane continuously. With increasing normalized chamber diameters, the effect of the confined wall decreases and the oscillation in the chamber weakens, as shown in Figure 15. Above of all, the radial deflective oscillation in CIJR is originally caused by the natural instability of the jets and the impinging instability in the impingement region, but is self-sustained by the interaction between the impingement plane and the confined wall of chamber.

The cause of axial random oscillation and vortex shedding

The third issue is the causes of the axial oscillation and vortex shedding appearing at $Re > 200$. Unlike the stagnation point offset of unconfined opposed jets, the axial instability in CIJR is pronounced, and this difference should be ascribed to the effects of the nozzle separation and the confined boundary. Our previous studies about the instability of axisymmetric and unconfined opposed jets indicate that there exists a range of $2 \le L/d \le 8$, in which the stagnation point is very sensitive to the exit velocity fluctuation.[25,26] The nozzle separations of $L/d = 4.8$ and 6.67 used in CIJR are the most unstable nozzle separations in the range of $2 \le L/d \le 8$, at which the locations of the impingement planes are very sensitive to the axial velocity fluctuation. With the increasing *Re*, the axial fluctuations in the inlets of the opposed jets increase, and instantaneous momentum imbalance will cause the axial movement of the impingement plane, which will enhance the interaction between the impingement plane and the confined chamber wall and induce an axial oscillation of the impingement plane conversely.

As *Re* increases to 1000 or more, the axial fluctuations in the inlets of the opposed jets increase and have even higher frequencies. From the results in our previous study,[29] the impingement plane of axisymmetric opposed jets only synchronizes with low-frequency disturbance. So the axial oscillation in CIJR at $Re > 1000$ tends to become the stagnation point offset, as shown in Figures 7 and 8. Even though the high frequency disturbance in the jet inlets does not cause obvious axial oscillation, it results in antisymmetric waves and vortex streets on the impingement plane, as shown in Figure 7. The vortex shedding tears and destroys the impingement plane and enhances the fluid mixing largely.

Conclusions

In order to successfully exploit opposed jets for engineering applications, it is very necessary to study the flow regimes in CIJR. In current study, the flow regimes in CIJR were experimentally investigated at $100 \le Re \le 2000$ and $2 \le D/d \le 12$. Results show that with increasing *Re*, a segregated flow

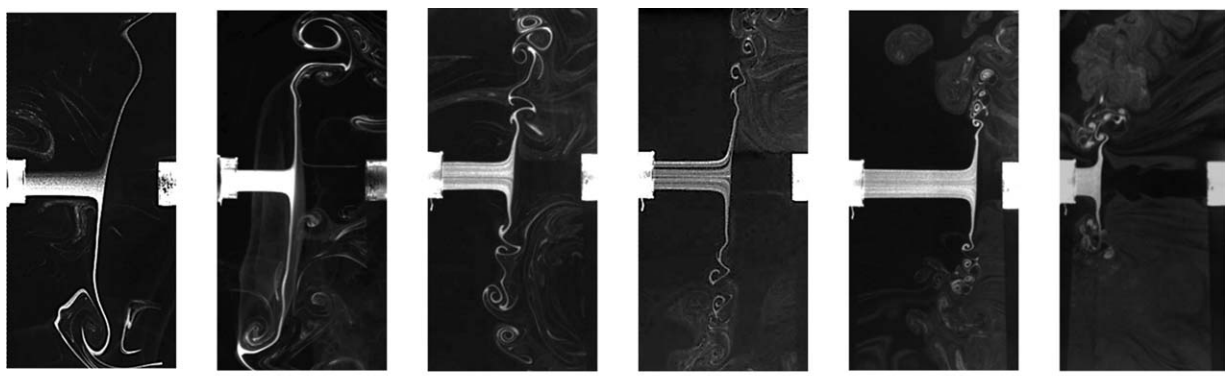

(a) *Re*=100 (b) *Re*=200 (c) *Re*=300 (d) *Re*=500 (e) *Re*=1000 (f) *Re*=2000

Figure 18. Typical snapshots by CCD camera of unconfined opposed jets at *L* = 4.8*d*.

regime, a self-sustained deflective oscillation and a combination of vortex shedding and axial instability emerge in turns in the CIJR. With the increase of *Re* to 500, the flow in CIJR undergoes a transition from a radial deflective oscillation to an axial instability. The onset and the evolution of the natural instability of the jets and the impinging instability in the impingement region are the origins of the radial deflective oscillation, while it is self-sustained by the interaction between the impingement plane and the confined chamber wall in CIJR. The sensitive nozzle separation, the increasing perturbance in the jets with *Re* and the confined boundary are the causes of the axial instability in CIJR. The synchronous occurrences of radial deflective oscillation and axial oscillation are the main cause of the complex and chaotic flow in CIJR.

The results in current study present a significant contribution to the knowledge of the intrinsic mechanism in CIJR, which are important to its design and scale-up. The results will also provide a sound basis for the future CFD simulation and stability analysis of flow regimes in CIJR.

Acknowledgments

This study was supported by the National Development Programming of Key Fundamental Researches of China (2010CB227004). Especially, authors express sincere thanks to the anonymous reviewers for their helpful suggestions on the quality improvement of the article.

Notation

d = jet diameter or nozzle inner diameter
D = chamber diameter
L = nozzle separation of free opposed jets
h = height from nozzle plane to the dome
I = intermittency factor
rms = root mean square
Re = jet Reynolds number
St = Strouhal number
t, t_0, t_d = time
u_0 = bulk mean velocity
x, y, z = axial, radial coordinates
ρ = air density
μ = dynamic viscosity of air
θ_1, θ_2, θ_3 = deflective angle

Literature Cited

1. Tamir A. Impinging Streams Reactors: Fundamentals and Applications. Amsterdam: Elsevier, 1994.
2. Kolodziej P, Macosko CW, Ranz WE. The effect of impingement mixing on striation thickness distribution and properties in fast polyurethane polymerisation. *Polym Eng Sci*. 1982;22:388–392.
3. Kolodziej P, Yang WP, Macosko CW, Wellinghoff ST. Impingement mixing and its effect on the microstructure of RIM polyurethanes. *J Polym Sci*. 1986;25:2359–2377.
4. Johnson BK, Prud'homme RK. Chemical processing and micromixing in confined impinging jets. *AIChE J*. 2003;49:2264–2282.
5. Santos RJ, Sultan MA. State of the art of mini/micro jet reactors. *Chem Eng Tech*. 2013;36:937–949.
6. Wood PE, Hrymak A, Yeo R, Johnson DA, Tyagi A. Experimental and computational studies of the fluid mechanics in an opposed jet mixing head. *Phys Fluids A*. 1991;3:1362–1368.
7. Johnson DA, Wood PE. Self-sustainable oscillations in opposed impinging jets in an enclosure. *Can J Chem Eng*. 2000;78:867–875.
8. Teixeira AM, Santos RJ, Costa MRPFN, Lopes JCB. Hydrodynamics of the mixing head in RIM: LDA flow-field characterization. *AIChE J*. 2005;51:1608–1619.
9. Santos RJ, Erkoç E, Dias MM, Teixeira AM, Lopes JCB. Hydrodynamics of the mixing chamber in RIM: PIV flow-field characterization. *AIChE J*. 2008;54:1153–1163.
10. Santos RJ, Erkoç E, Dias MM, Lopes JCB. Dynamic behavior of the flow field in a RIM machine mixing chamber. *AIChE J*. 2009;55:1338–1351.
11. Santos RJ, Teixeira AM, Lopes JCB. Study of mixing and chemical reaction in RIM. *Chem Eng Sci*. 2005;60:2381–2398.
12. Li X, Santos RJ, Lopes JCB. Modelling of self-induced oscillations in the mixing head a RIM machine. *Can J Chem Eng*. 2007;85:45–54.
13. Schütz S, Bierdel M, Piesche M. Charakterisierung des mischverhaltens von gegenstrom-injektions-mischern. *Chem Ing Tech*. 2005;77:398–405.
14. Bierdel M, Piesche M. CFD-simulation and experimental investigation of impingement mixing in reaction injection molding (RIM). In: 3rd European Congress of Chemical Engineering. Nuremberg, 26–28 June, 2001.
15. Fonte CP, Santos RJ, Dias MM, Lopes JCB. Quantification of mixing in RIM using a non-diffusive two-phase flow numerical model. *Int J Chem React Eng*. 2011;9:A114.
16. Liu Y, Fox RO. CFD predictions for chemical processing in a confined impinging-jets reactor. *AIChE J*. 2006;52:731–744.
17. Icardi M, Gavi E, Marchisio DL, Barresi AA, Olsen MG, Fox RO, Lakehal D. Investigation of the flow field in a three-dimensional Confined Impinging Jets Reactor by means of microPIV and DNS. *Chem Eng J*. 2011;166:294–305.
18. Gavi E, Marchisio DL, Barresi AA. CFD modelling and scale-up of Confined Impinging Jet Reactors. *Chem Eng Sci*. 2007;62:2228–2241.
19. .Nakamura S. Brodkey RS. Direct and large eddy simulation of the three-dimensional unsteady flows in the counter-jet mixing vessel. In: ASME Fluids Engineering Summer Conference. Boston, Massachusetts, 11–15 June, 2000.
20. Siddiqui SW, Zhao Y, Kukukova A, Kresta SM. Characteristics of a confined impinging jet reactor: Energy dissipation, homogeneous and heterogeneous reaction products, and effect of unequal flow. *Ind Eng Chem Res*. 2009;48:7945–7958.
21. Zhao Y, Brodkey RS. Averaged and time-resolved, full-field (three-dimensional), measurements of unsteady opposed jets. *Can J Chem Eng*. 1998;76:536–545.
22. Unger DR, Muzzio FJ. Laser-induced fluorescence technique for the quantification of mixing in impinging jets. *AIChE J*. 1999;45:2477–2486.
23. Devahastin S, Mujumdar AS. A numerical study of flow and mixing characteristics of laminar confined impinging streams. *Chem Eng J*. 2002;85:215–223.
24. Pawlowski RP, Salinger AG, Shadid JN, Mountziaris TJ. Bifurcation and stability analysis of laminar isothermal counterflowing jets. *J Fluid Mech*. 2006;551:117–139.
25. Li WF, Sun ZG, Liu HF, Wang FC, Yu ZH. Experimental and numerical study on stagnation point offset of turbulent opposed jets. *Chem Eng J*. 2008;138:283–294.
26. Li WF, Yao TL, Wang FC. Study on factors influencing stagnation point offset of turbulent opposed jets. *AIChE J*. 2010;56:2513–2522.
27. Li WF, Yao TL, Liu HF, Wang FC. Experimental investigation of flow regimes of axisymmetric and planar opposed jets. *AIChE J*. 2011;57:1434–1445.
28. Li WF, Huang GF, Tu GY, Liu HF, Wang FC. Experimental study of planar opposed jets with acoustic excitation. *Phys Fluids*. 2013;25:014108.
29. Li WF, Huang GF, Tu GY, Liu HF, Wang FC. Experimental study of oscillation of axisymmetric turbulent opposed jets with modulated airflow. *AIChE J*. 2013;59:4828–4838.
30. O'Neill P, Soria J, Honnery D. The stability of low Reynolds number round jets. *Exp Fluids*. 2004;36: 473–483.
31. Crow SC, Champagne FH. Orderly structure in jet turbulence. *J Fluid Mech*. 1971;48:547–591.
32. Rockwell D, Naudascher E. Self sustained oscillations of impinging free shear layer. *Ann Rev Fluid Mech*. 1979;11:67–94.
33. Varieras D, Brancher P, Giovannini A. Self-sustained oscillations of a confined impinging jet. *Flow Turbul Combust*. 2007;78:1–15.
34. Villermaux E, Hopfinger EJ. Self-sustained oscillations of a confined jet: a case study for the non-linear delayed saturation model. *Physica D*. 1994;72:230–243.

Manuscript received Nov. 26, 2013, and revision received Feb. 5, 2014.